Arabian Journal of Chemistry (2022) **15**, 103568

King Saud University

Arabian Journal of Chemistry

www.ksu.edu.sa
www.sciencedirect.com

ORIGINAL ARTICLE

Improved anti-inflammatory and anticancer properties of celecoxib loaded zinc oxide and magnesium oxide nanoclusters: A molecular docking and density functional theory simulation

Nabo Sun [a], Mohammad Javed Ansari [b,*], Andrew Ng Kay Lup [c], Masoud Javan [d], Alireza Soltani [e,*], Seyed Reza Khandoozi [f], Ali Arian Nia [f,*], Samaneh Tavassoli [e,*], Md Lutfor Rahman [g,*], Mohd Sani Sarjadi [g], Shaheen M. Sarkar [h], Chia-Hung Su [i,*], Hoang Chinh Nguyen [j]

[a] *College of Biology and Environment Engineering, Zhejiang Shuren University, Hangzhou, Zhejiang, 310015, China*
[b] *Department of Pharmaceutics, College of Pharmacy, Prince Sattam Bin Abdulaziz University, Al-kharj, Saudi Arabia*
[c] *School of Energy and Chemical Engineering, Xiamen University Malaysia, Jalan Sunsuria, Bandar Sunsuria, 43900 Sepang, Selangor Darul Ehsan, Malaysia*
[d] *Department of Physics, Faculty of Sciences, Golestan University, Gorgan, Iran*
[e] *Golestan Rheumatology Research Center, Golestan University of Medical Science, Gorgan, Iran*
[f] *Cancer Research Center, Golestan University of Medical Sciences, Gorgan, Iran*
[g] *Faculty of Science and Natural Resources, Universiti Malaysia Sabah, 88400 Kota Kinabalu, Sabah, Malaysia*
[h] *Department of Applied Science, Technological University of the Shannon, Moylish Park, Limerick V94 EC5T, Ireland*
[i] *Department of Chemical Engineering, Ming Chi University of Technology, New Taipei City, Taiwan*
[j] *Faculty of Applied Sciences, Ton Duc Thang University, Ho Chi Minh City 700000, Viet Nam*

Received 8 July 2021; accepted 10 November 2021
Available online 15 November 2021

KEYWORDS

$Zn_{12}O_{12}$;
$Mg_{12}O_{12}$;
Celecoxib;
Adsorption mechanism;
Optoelectronic properties

Abstract Present study offers great prospects for the adsorption of anti-inflammatory celecoxib molecule (CXB) over the surface of zinc oxide ($Zn_{12}O_{12}$) and magnesium oxide ($Mg_{12}O_{12}$) nanoclusters in several environments by performing robust theoretical calculations. Density functional theory (DFT), time-dependent density functional theory (TDDFT) and molecular docking calculations have been extensively carried out to predict the foremost optimum site of CXB adsorption. It has been observed that the CXB molecule prefers to be adsorbed by its SO_2 site on the Zn-O and Mg-O

* Corresponding Authors.
E-mail addresses: mj.ansari@psau.edu.sa (M. Javed Ansari), alireza.soltani@goums.ac.ir (A. Soltani), Drkhandoozi92002@yahoo.com (S. Reza Khandoozi), aliariannia@gmail.com (A. Arian Nia), tavassolisam54@gmail.com (S. Tavassoli), lotfor@ums.edu.my (M. Lutfor Rahman), chsu@mail.mcut.edu.tw (C.-H. Su).

Peer review under responsibility of King Saud University.

Production and hosting by Elsevier

https://doi.org/10.1016/j.arabjc.2021.103568
1878-5352 © 2021 The Author(s). Published by Elsevier B.V. on behalf of King Saud University.
This is an open access article under the CC BY-NC-ND license (http://creativecommons.org/licenses/by-nc-nd/4.0/).

bonds of the $Zn_{12}O_{12}$ and $Mg_{12}O_{12}$ nanoclusters instead of NH_2 and NH sites, where electrostatic interactions dominate over the bonding characteristics of the conjugate complexes. Furthermore, the presence of interactions between the CXB molecule and nanoclusters has also been evidenced by the UV–Vis absorption spectra and IR spectra. Molecular docking analysis has revealed that both adsorption states including CXB/$Zn_{12}O_{12}$ and CXB/$Mg_{12}O_{12}$ have good inhibitory potential against protein tumor necrosis factor alpha (TNF-α) and Interleukin-1 (IL-1), and human epidermal growth factor receptor 2 (HER2). Hence they might be explored as efficient TNF-α, IL-1, and HER2 inhibitors. Hence from the study, it can be anticipated that these nanoclusters can behave as an appropriate biomedical carrier for the CXB drug delivery.

© 2021 The Author(s). Published by Elsevier B.V. on behalf of King Saud University. This is an open access article under the CC BY-NC-ND license (http://creativecommons.org/licenses/by-nc-nd/4.0/).

1. Introduction

Nanocarrier emergence in drug delivery systems has significantly improved the solubility, stability and chemotherapeutic effects of drug by reducing its toxicity (Fakhar et al., 2017; Cao et al., 2021a; Cao et al., 2021b). Among a wide variety of nanocarriers in the field of nanomaterials, magnetic and nanoelectronic, metal oxides have been extensively used in the area of biomedicine including gene delivery, cancer therapy, bio-imaging and drug delivery (Hassanian et al.; Javan; Zhang et al., 2016; Zhang et al., 2021; Yang et al., 2021; Zhao and Guo, 2021; Deng et al., 2021; Sharma et al., 2020; Chen et al., 2020). Good biocompatibility, non-toxicity, high stability and selectivity of ZnO and MgO make them potential candidates for bio-imaging and drug delivery (Li et al., 2018; Cai et al., 2016). Moreover, anti-microbial and anti-inflammatory properties of these n-type semiconductors, i.e. ZnO and MgO nanoparticles broaden their biomedical application related to skin inflammation (Lin et al., 2019; Alalaiwe et al., 2019; Ansari, 2017).

In recent studies, various nanoclusters of ZnO and MgO have been explored as efficient drug carrier via adsorption of different biomolecules and drug molecules (Krishnamoorthy et al., 2012; Malarkodi et al., 2014). For instance, the encapsulation of 2-methoxyestradiol into MgO nanoparticles modified with the polymer polyethylene glycol were used for anticancer prostate therapy (Alfaro et al., 2019). Furthermore, photophysical and electronic properties of DNA nucleotide conjugated $(ZnO)_3$ cluster had also been studied by Kumari *et al.* in aqueous phase using density functional theory (DFT) and time dependent-density functional theory (TDDFT) method (Kumari et al., 2019). Moreover, Tayebee and co-workers investigated the adsorption of some aliphatic aldehydes on the $Zn_{12}O_{12}$ nanocage and revealed the significant reduction in the adsorption energy and changes in the electronic properties which indicated $Zn_{12}O_{12}$ nanocage as an efficient sensor for toxic formaldehyde (Tayebee et al., 2015).

Fallahi et al. (2018) have explored a variety of nanocages including $Al_{12}N_{12}$, $Al_{12}P_{12}$, $B_{12}N_{12}$, $Be_{12}O_{12}$, $C_{12}Si_{12}$, $Mg_{12}O_{12}$ and C_{24} towards the detection as well as adsorption of tabun molecule using DFT studies and observed that $Mg_{12}O_{12}$ nanocluster was the best candidate for tabun adsorption without any chemical change in its structure whereas $Al_{12}N_{12}$ behaves as a good sensor for it. In addition to drug carrier, ZnO nanoparticles are efficient and fast in drug release as well. Farmanzadeh and Keyhanian have theoretically observed an increase in the release of amantadine molecule from $Zn_{12}O_{12}$ in comparison with $B_{12}N_{12}$ nanocage because of low binding energy in aqueous phase (Farmanzadeh and Keyhanian, 2019). Zhao *et al.* reported the role of ZnO nanoparticle capsules for loading isotretinoin with a capacity as high as 34.6 wt% and showed at low pH (below 6), ZnO-Isotretinoin decomposed quickly and more than 90% of the drug was released within 8 h (Zhao et al., 2017). Ravaei *et al.* showed the strong interaction of isoniazid (INH) drug via its nitrogen and oxygen atoms to the Mg atoms of the $Mg_{12}O_{12}$, while the electronic properties of the nanocage was not significantly changed (Ravaei et al., 2019).

Celecoxib (CXB) is a well-known nonsteroidal anti-inflammatory drug which is commonly prescribed to relieve pain and inflammation. CXB inhibits the transformation of arachidonic acid to prostaglandin precursors by blocking the enzyme cyclooxygenase, which result in decreasing the prostaglandins and hence acts as antipyretic, analgesic and anti-inflammatory (Mandracchia et al., 2016). In addition, CXB has also been considered as an effective drug to prevent the development of sporadic adenomatous polyps, precursors of colorectal cancer (Alamdarsaravi et al., 2017). Cao *et al.* have shown the naproxen loaded with OH-$B_{12}N_{12}$ was able to inhibit both IL-1 receptor and TNF-α receptor targets in comparison to $B_{12}N_{12}$ and $B_{12}P_{12}$ systems (Cao et al., 2021). To the best knowledge of the authors, the adsorption of CXB drug molecule on $Zn_{12}O_{12}$ and $Mg_{12}O_{12}$ metal clusters was not explored for biomedical applications. Thus, in this study, metal-oxide nanoclusters i.e. $Zn_{12}O_{12}$ and $Mg_{12}O_{12}$ have been theoretically explored for the adsorption of CXB drug molecule. By using DFT, TDDFT and molecular docking calculations, the attempt to design an effective drug carrier for CXB was made through the utilization of the unique properties of such metal oxide nanoclusters.

2. Computational details

All theoretical calculations including geometry optimization, interaction energies, frontier molecular orbitals (FMO) and transition state (TDDFT) studies of pristine and CXB adsorbed metal oxide nanoclusters ($Zn_{12}O_{12}$ and $Mg_{12}O_{12}$) were performed using B3LYP and B3PW91 functionals with Gaussian 09 suite of program (Gaussian et al., 2009). In all cases, 6-311 g(d,p) basis set was chosen for H, C, N, O, F and S atoms while LANL2DZ effective core potential (ECP) was chosen for Zn atoms. In order to evaluate the total density

of state (TDOS), the projected density of state (PDOS) and shaded surface map with projection of electron density plots Multiwfn 3.3.9 were done (Lu and Chen, 2012). Furthermore, the effect of solvent i.e. water, was also examined by implementing polarizable continuum model (PCM) as the solvation model to mimic the biological environment. To compute total energy and electron density, the SCF (self-consistent field) convergence limit was set to 1.0×10^{-6} a.u. All computations were fully relaxed with the relaxation criteria (RMS force = 0.0003, Max. force = 0.00045, RMS displacement = 0.0012, and max. displacement = 0.0018). The adsorption energies (E_{ads}) of CXB on metal oxide nanoclusters were calculated using the formula:

$$E_{ads} = E_{CXB/nanocluster} - (E_{nanocluster} + E_{CXB}) + E_{BSSE} \quad (1)$$

where $E_{CXB/nanocluster}$ is the total energy of the adsorption complex, $E_{nanocluster}$ is the total energy of the perfect metal-oxide nanocluster and E_{CXB} is the total energy of CXB molecule. The adsorption energies were corrected by adding basis set superposition error (BSSE) which accounts for the incompleteness of basis set in the calculation of weak intermolecular interactions by implementing the counterpoise method. Quantum molecular descriptors of CXB, nanoclusters and adsorption complexes were calculated to predict their respective physicochemical properties (Soltani et al., 2018; Soltani et al., 2014):

$$\mu = -\frac{1}{2}(I + A) \quad (2)$$

$$\chi = -\mu \quad (3)$$

$$\eta = \frac{1}{2}(I - A) \quad (4)$$

$$S = \frac{1}{2\eta} \quad (5)$$

$$\omega = \frac{\mu^2}{2\eta} \quad (6)$$

where ionization potential, electron affinity, electronegativity, global hardness, global softness, chemical potential and electrophilicity index are I, A, χ, η, S, μ and ω respectively. The values of I and A were respectively defined as negative orbital energies of the HOMO (highest occupied molecular orbital), $-E_{HOMO}$, and the LUMO (lowest unoccupied molecular orbital), $-E_{LUMO}$, based on Koopmans' approximation.

Molecular docking simulations were calculated by the Auto Dock software (4.2) (Morris et al., 2009). Three-dimensional structures of TNF-alpha (PDB ID: 2AZ5), HER2 kinase (PDB ID: 3RCD), and IL1A-S100A13 complexes (PDB ID: 2L5X) were retrieved from Protein Data Bank. Protein files for docking were created via cognate ligand removal; non-polar hydrogen atoms, polar hydrogen atoms and the Kollman atom partial charges were added by the Auto Dock Tools (ADT). Lamarckian genetic algorithm was used for local search method. A grid box of 60x60x60 with a spacing of 0.375 Å was created for preparation of autogrid (Mirzaei et al., 2017a; Mirzaei et al., 2017b). A total of 100 GA runs were performed for docking. Maestro 11.0 Schrodinger program was used for preparation of 2D and 3D presentation.

3. Result and discussion

3.1. Structural analysis of CXB loaded $Zn_{12}O_{12}$/$Mg_{12}O_{12}$

The relaxed structural parameters of Celecoxib drug on $Zn_{12}O_{12}$ and $Mg_{12}O_{12}$ nanoclusters were calculated by the B3LYP and B3PW91 methods for both vacuum and aqueous environments and the optimized structures were shown in Figs. 1, 2, 3 and 4. The lengths of Zn-O, O_1-S, N_3-S, N_1-C_3, N_1-N_2, and C_4-F bonds for the $Zn_{12}O_{12}$ and CXB were computed to be 1.983, 1.461, 1.694, 1.393, 1.421 and 1.346 Å by the B3LYP functional and 1.983, 1.463, 1.670, 1.384, 1.408 and 1.356 Å by the B3PW91 functional and the studies represent good agreement with the experimental and theoretical results (Pulay et al., 1983; Vijayakumar et al., 2016). Farmanzadeh and Keyhanian have shown the interaction of amantadine drug with $Zn_{12}O_{12}$ nanocluster and reported two types of Zn–O bonds with the values of 1.89 and 1.98 Å by the PBE functional (Li et al., 2018). The Zn-O-Zn angles increase from 87.22° in pure $Zn_{12}O_{12}$ to 88.30° and 87.63° in State I and II within the water phase also there have been not many changes in other scenarios. O-S-O angles for the State I (121.72°) and II (119.09°) in vacuum phase observed more changes than any other scenario while in the aqueous phase are 115.39° and 113.08°. The geometry of $Zn_{12}O_{12}$ nanocluster is made of six 4-MRs (four-membered rings) with the symmetry of T_h (Baei et al., 2013). Fig. 1 represents HOMO orbital of CXB drug which is more distributed on the C-C and C-N bonds in aromatic and pyrazole rings and LUMO orbital which is more localized on the C-C bonds in aromatic ring.

To better perceive the adsorption behavior of CXB with $Zn_{12}O_{12}$ and $Mg_{12}O_{12}$ nanoclusters, we evaluated various orientations of the CXB through –NH_2 and –SO_2 groups by changing their separation distances on $Zn_{12}O_{12}$ and $Mg_{12}O_{12}$ surfaces. As depicted in Figs. 3 and 4, CXB drug in relaxed structures indicate the best trend for the interaction with the electrophilic Zn and Mg atoms of nanoclusters as compared with other positions through its O atom as the nucleophilic agent; this result is in agreement with MEP plots. In comparison between Tables 1 and 2, the E_{ads} values and separation distance (BD) of CXB in the most stable state (State II) on the $Zn_{12}O_{12}$ surface were −1.18 eV (2.10 Å) in vacuum environment and −1.38 eV (2.02 Å) in solvent environment by the B3PW91 functional, while for the B3LYP functional were −1.20 eV (2.10 Å) in vacuum environment and −1.26 eV (2.10 Å) in solvent environment, respectively. In contrast with $Zn_{12}O_{12}$, the adsorption process of CXB through the sulphonamide (III: SO_2NH_2) group demonstrates a strong hybridization in vacuum environment due to a strong covalent interaction between the CXB and the adsorbent in comparison to amino (IV: NH_2) group of the drug. E_{ads} and BD values related to B3LYP functional in the most stable state (State III) indicate strong binding state for the CXB on the Mg atom rather than O atom of the $Mg_{12}O_{12}$ with the amount of −1.87 eV and 2.07 Å respectively.

The stability of CXB through the amino (NH_2) group (State IV) in solvent environment is spontaneous and it could be increased due to the negative values of solvation energy (E_{sol}) as the E_{ads} and BD values were calculated to be −2.08 eV and 2.25 Å, respectively. On the other hand, BD value from CXB to the nanoclusters seems to remarkably

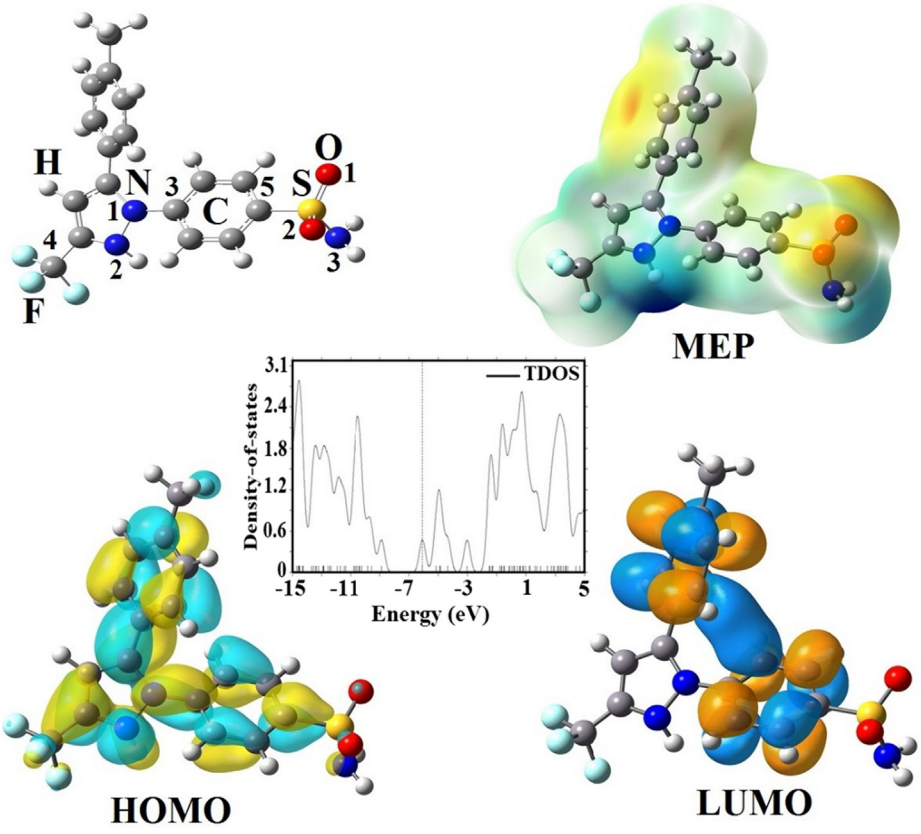

Fig. 1 Optimized structures, FMO and TDOS plots of CXB.

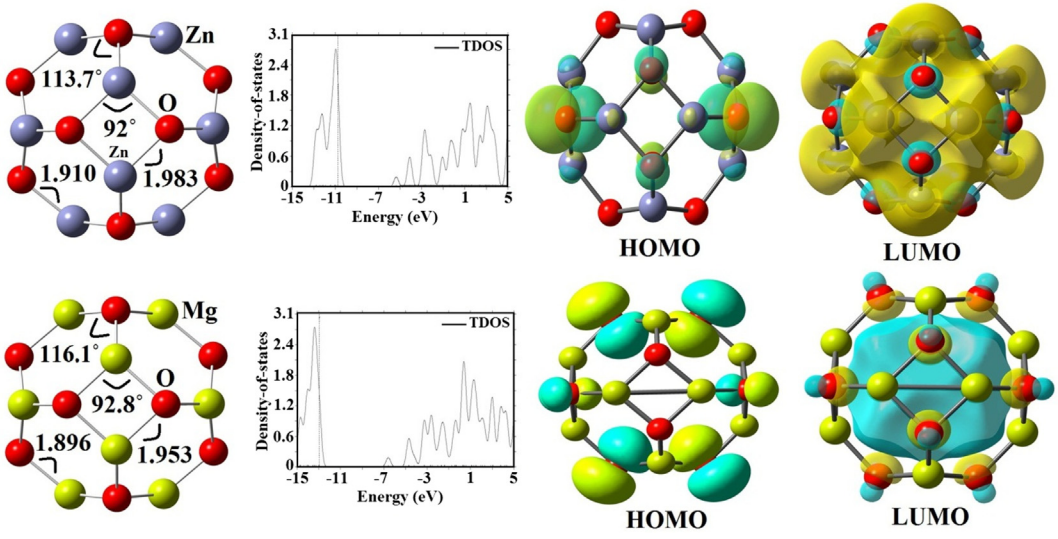

Fig. 2 Optimized structures, FMO and TDOS plots of $Zn_{12}O_{12}$ and $Mg_{12}O_{12}$ nanoclusters.

depend on the orientation of drug and curvature of the clusters. Lower E_{ads} values represent that the CXB adsorption on the $Zn_{12}O_{12}$ in comparison with $Mg_{12}O_{12}$ becomes weak; therefore, drug with a non-covalent interaction is often separated from the adsorbent and can be delivered into target site (Chen et al., 2020; Abd El-Mageed, 2020). The adsorption behavior of isoniazid drug over the surface of $Mg_{12}O_{12}$ nanocluster has been reported by Lin et al. (2019) and feasible adsorption between the N and O atom of drug with Mg atom of complex has been demonstrated on the basis of negative value of adsorption energy i.e. −0.96 to −2.58 eV based on the dispersion corrected M062X level of theory. As shown in Fig. 5, shaded surface map with projection of electron density (SPE) plot demonstrates that the celecoxib could adsorbed on

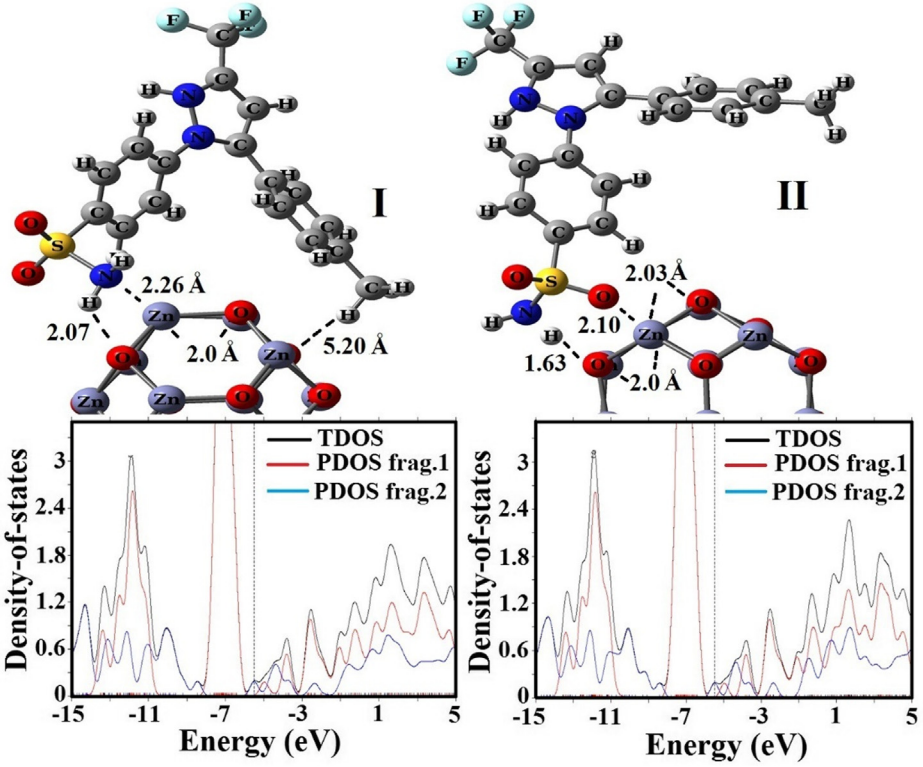

Fig. 3 Optimized structures and PDOS plots of CXB on the surface of $Zn_{12}O_{12}$ fullerene.

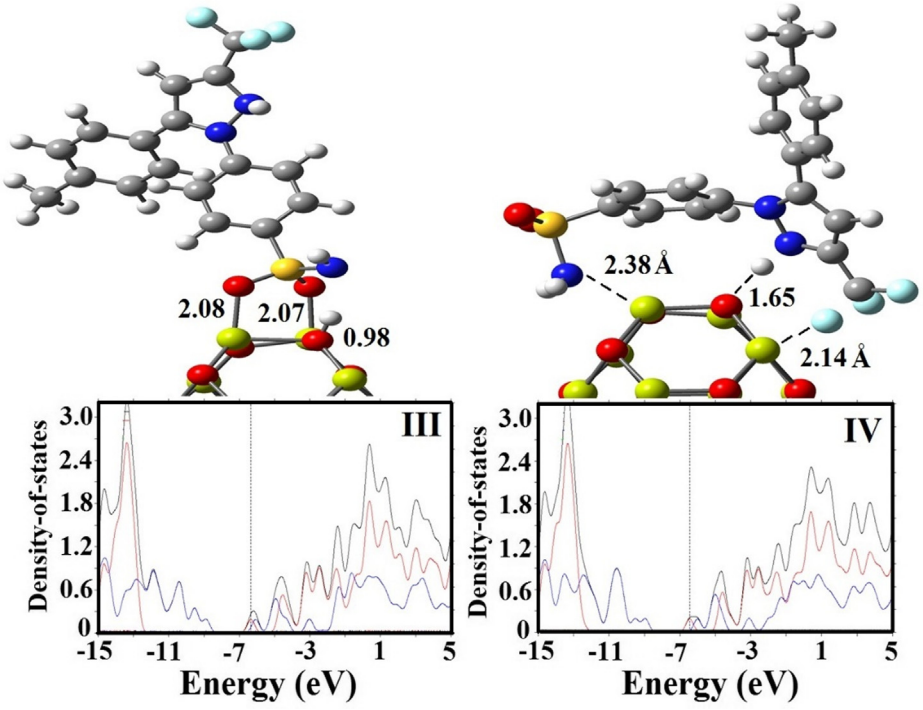

Fig. 4 Optimized structures and PDOS plots of CXB on the surface of $Mg_{12}O_{12}$ fullerene.

the surface of $Zn_{12}O_{12}$ fullerene through electrostatic interaction in nature (Ansari et al., 2014a; Ansari et al., 2014b). Table 1 and 2 demonstrate that the CXB through NH_2 group (I: 19.38 Debye at B3LYP and 16.53 Debye at B3PW91) in solvent environment has a higher value of dipole moment (DM) in comparison with the SO_2NH_2 group (II: 14.01 Debye at

Table 1 Computational results for CXB-$Zn_{12}O_{12}$ adsorption complexes in vacuum and aqueous environments using B3LYP/6–311 g (d,p) method.

Property		Vacuum			Aqueous	
	$Zn_{12}O_{12}$	I	II	$Zn_{12}O_{12}$	I	II
E_{HOMO} (eV)	−6.95	−4.35	−4.24	−5.96	−3.92	−3.92
E_{LUMO} (eV)	−2.80	−2.69	−2.70	−1.58	−1.70	−1.63
E_g (eV)	4.15	1.66	1.54	4.38	2.22	2.29
ΔE_g (%)	–	60.0	62.9	–	49.3	47.7
E_{ads} (eV)	–	−0.98	−1.20	–	−1.03	−1.26
BD (Å)	–	2.26	2.10	–	2.08	2.02
DM (Debye)	0.00	3.696	2.694	0.00	19.38	14.01
E_F (eV)	−4.88	−3.52	−3.47	−3.77	−2.81	−2.77
I (eV)	6.95	4.35	4.24	5.96	3.92	3.92
A (eV)	2.80	2.69	2.70	1.58	1.70	1.63
μ(eV)	−4.88	−3.52	−3.47	−3.77	−2.81	−2.78
χ(eV)	4.88	3.52	3.47	3.77	2.81	2.78
η(eV)	2.08	0.83	0.77	2.19	1.11	1.15
$S(eV^{-1})$	0.24	0.60	0.65	0.23	0.45	0.44
ω(eV)	5.73	7.46	7.82	3.24	3.56	3.36

Table 2 Computational results for CXB-$Zn_{12}O_{12}$ adsorption complexes in vacuum and aqueous environments using B3PW91/6–311 g (d,p) method.

Property		Vacuum		Aqueous		
	$Zn_{12}O_{12}$	I	II	$Zn_{12}O_{12}$	I	II
E_{HOMO} (eV)	7.00-	−4.36	−4.25	−6.00	−3.94	−3.97
E_{LUMO} (eV)	−2.61	−2.52	−2.53	−1.41	−1.47	−1.47
E_g (eV)	4.39	1.82	1.72	4.59	2.47	2.5
ΔE_g (%)	–	58.5	60.8	–	46.2	45.5
E_{ads} (eV)	–	−0.94	−1.18	–	−1.21	−1.38
BD (Å)	–	2.26	2.10	–	2.08	2.02
DM (Debye)	0.0	3.761	2.851	0.00	16.53	14.66
E_F (eV)	4.805-	3.44-	3.39-	−3.705	−2.705	−2.72
I (eV)	7.00	4.36	4.25	6.00	3.94	3.97
A (eV)	2.61	2.52	2.53	1.41	1.47	1.47
μ(eV)	−4.81	−3.44	−3.39	−3.71	−2.71	−2.72
χ(eV)	4.81	3.44	3.39	3.71	2.71	2.72
η(eV)	2.20	0.92	0.86	2.30	1.24	1.25
$S(eV^{-1})$	0.23	0.54	0.58	0.22	0.40	0.40
ω(eV)	5.26	6.43	6.68	2.99	2.96	2.96

B3LYP and 14.66 Debye at B3PW91). The higher DM value demonstrates the higher complex reactivity. In a physiological medium, significant increment in DM value indicates enhanced solubility which is an acceptable characteristic for drug delivery systems (Dastani et al., 2021).

Infrared (IR) spectroscopy has also been employed to study the possibility of molecular interactions of CXB with $Zn_{12}O_{12}$ and $Mg_{12}O_{12}$ nanoclusters by the B3LYP functional. Theoretical IR spectrum of $Mg_{12}O_{12}$ demonstrates the band at 656 cm^{-1} strongly corresponded to Mg-O stretching vibration (Moorthy et al., 2015). Theoretical IR spectrum of $Zn_{12}O_{12}$ exhibits bands at 465, 552, 584, and 644 cm^{-1} corresponded to Zn–O stretching vibration (Aggarwal, 2006; Wahab et al., 2009). The IR spectrum of State I demonstrated characteristic bands at 1038 and 3338 cm^{-1} that are attributed to N–H stretching vibration of SO_2NH_2 group and 1293 and 1527 cm^{-1} for S = O asymmetric and symmetric stretching, and 1202 cm^{-1} for C–F stretching. In contrast, IR spectrum of State II exhibited characteristic bands at 1066 and 3667 cm^{-1} that are assigned to N–H stretching vibration of SO_2NH_2 group and 1254 cm^{-1} for C–F stretching, and S = O asymmetric and symmetric stretching are distributed to 1271 and 1482 cm^{-1}. These results were in good agreement with the experimental data obtained by He and co-authors (He et al., 2017).

3.2. Electronic properties of CXB-$Zn_{12}O_{12}$ and CXB-$Mg_{12}O_{12}$

The values of energy gap (E_g), Fermi level (E_F), and change of energy gap (ΔE_g) for CXB, $Zn_{12}O_{12}$ and $Mg_{12}O_{12}$, and considered complexes are summarized in Tables 1, 2 and 3. The E_g values for the $Zn_{12}O_{12}$ nanocluster in both vacuum and solvent

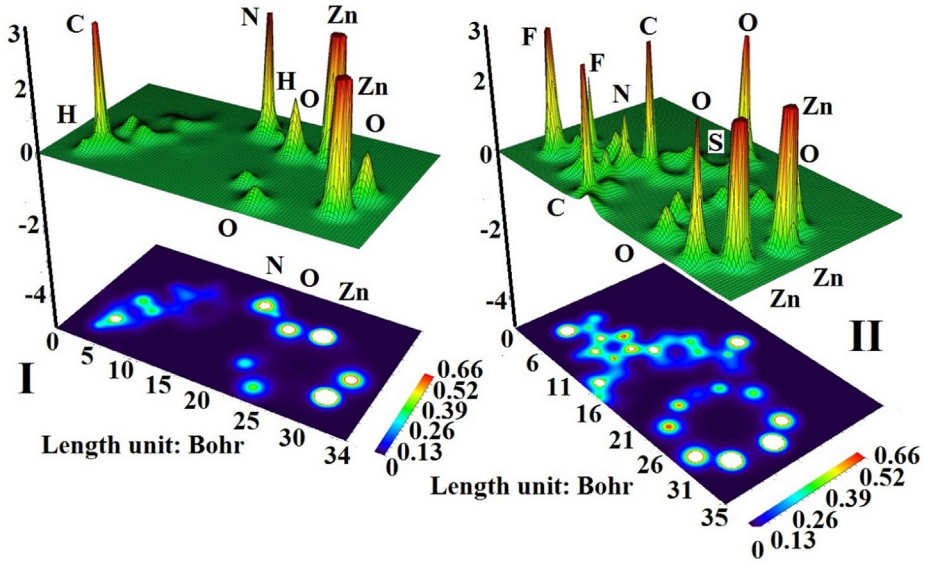

Fig. 5 SPE plots of the CXB adsorbed on the of $Zn_{12}O_{12}$ surface in State I and II.

phases were 4.15 and 4.38 eV by B3LYP functional and 4.39 and 4.59 eV by B3PW91 functional, whereas they reduce to 1.66 and 1.54 eV in vacuum phase and 2.22 and 2.29 eV in solvent phase for the State I and II respectively after CXB adsorption on $Zn_{12}O_{12}$ surface, which is close to the theoretical results by Ahmadi Peyghan et al. (2013), Ghenaatian et al. (2013). This represents that interaction of CXB with $Zn_{12}O_{12}$ induces some shifts in the electronic features and therefore E_g values were reduced when compared with both pure CXB and $Zn_{12}O_{12}$. The change in energy gap for the CXB-$Zn_{12}O_{12}$ complex in solvent phase is more than the vacuum phase. Similar E_g reduction trend was also observed in CXB-$Mg_{12}O_{12}$ complexes however the reduction effect was lesser as compared with the former. For CXB adsorbed on the $Zn_{12}O_{12}$ and $Mg_{12}O_{12}$ nanoclusters, PDOS of a complex appeared with small E_g in which each fragment (where the nanoclusters and CXB respectively were determined as frags1 and 2) has the electronic total density of state (TDOS) near the states of HOMO and LUMO (Figs. 3 and 4).

Tables 1, 2, and 3 represent the quantum molecular descriptors (QMDs) of CXB, $Zn_{12}O_{12}$, $Mg_{12}O_{12}$ and adsorption complexes. The interaction of $Zn_{12}O_{12}$ and $Mg_{12}O_{12}$ nanoclusters with CXB, a significant decrement in the E_g value has enabled a more facile electron transition thus increasing its reactivity for CXB interaction (Abdolahi et al., 2020; Soltani et al., 2022). QMDs of adsorption complexes also indicated that they are less electronegative and chemically softer. In terms of electrophilicity, CXB-$Zn_{12}O_{12}$ becomes more electrophilic while CXB-$Mg_{12}O_{12}$ becomes less electrophilic. These consequences demonstrated a notable change in the electronic properties of adsorption complexes as comparing to the pure $Zn_{12}O_{12}$ and

Table 3 Computational results for CXB-$Mg_{12}O_{12}$ adsorption complexes in vacuum and aqueous environments using B3LYP/6–311 g (d,p) method.

Property		Vacuum		Aqueous		
	$Mg_{12}O_{12}$	III	IV	$Mg_{12}O_{12}$	III	IV
E_H/eV	−6.58	−4.13	−4.02	−5.99	−4.0	−3.22
E_L/eV	−1.74	−1.66	−1.78	−1.03	−1.06	−1.11
E_g/eV	4.84	2.47	2.24	4.96	2.94	2.11
ΔE_g (%)	–	48.97	53.72	–	40.72	57.46
E_{ads}/eV	–	−1.87	−1.17	–	−1.90	−2.08
D/Å	–	2.07	2.38	–	2.14	2.25
DM/Debye	0.0	2.05	3.75	0.0	3.78	10.88
E_F/eV	−4.16	−2.89	−2.90	−3.51	−253	−2.17
I (eV)	6.58	4.13	4.02	5.99	4.00	3.22
A (eV)	1.74	1.66	1.78	1.03	1.06	1.11
μ(eV)	−4.16	−2.90	−2.90	−3.51	−2.53	−2.17
χ(eV)	4.16	2.90	2.90	3.51	2.53	2.17
η(eV)	2.42	1.24	1.12	2.48	1.47	1.06
S(eV^{-1})	0.21	0.40	0.45	0.20	0.34	0.47
ω(eV)	3.58	3.39	3.75	2.48	2.18	2.22

$Mg_{12}O_{12}$ nanoclusters, making them suitable for applications involving molecular sensor of high sensitivity.

3.3. Analysis of UV–visible spectra

We have calculated the UV–visible absorption spectra of CXB interaction with $Zn_{12}O_{12}$ and $Mg_{12}O_{12}$ nanoclusters in vacuum and aqueous phases using TDDFT/B3PW91 level of theory, as displayed in Tables 4 and 5. HOMOs and LUMOs that were involved in the electronic transitions were illustrated in Fig. 6. Table 4 represents the utmost values of E (vertical excitation energies), λ_{max} (excitation wavelength), and *f* (oscillator strength). The UV–vis spectra of pure $Zn_{12}O_{12}$ and $Mg_{12}O_{12}$ nanoclusters reveal existence of one main maximum band with λ_{max} at 251.06 and 252.78 nm and therefore the E values of 4.938 and 4.909 eV in the aqueous environment respectively. Sharma *et al*. reported the absorption band of the synthesized ZnO nanoparticles with a λ_{max} at 270.5 nm (Sharma et al., 2018); which is close to our theoretical calculations. Moazzen and co-workers experimentally have shown the UV–visible absorption spectra of the ZnO nanoparticles with a band at 317 nm (3.30 eV) by dispersing the powder in deionized water (Moghri Moazzen et al., 2012).

UV–visible absorption spectra for the pure CXB represents four maximum absorption bands with the λ_{max} value of 260 (4.768 eV), 294 (4.214 eV), 354 (3.498 eV) and 470 nm (2.635 eV) which are in agreement with theoretical (Abdolahi et al., 2018) and experimental (Revathi et al., 2011) reports. The UV–visible absorption spectra demonstrate that the strong interaction of CXB through its $-NH_2$ group with $Zn_{12}O_{12}$ and $Mg_{12}O_{12}$ nanoclusters leading to the optical changes compared to $-SO_2$ group of the drug because of the electronic transitions between the non-bonding *p*-orbital of nitrogen and the unoccupied *sp*-hybrid orbitals of zinc and magnesium atoms (Nagare et al., 2017). The maxima absorbance band in the State I and III were observed at 346.11 nm (*f*: 0.2049) and 390.14 nm (*f*: 0.1991) which were superimposed on the absorption band of CXB. The maxima absorbance bands in the State I and III occurred at longer wavelengths with the main electron transitions in solvent phase as H → L + 1 (71%) and H-1 → L (68%) respectively.

3.4. Molecular docking studies of CXB loaded with $Zn_{12}O_{12}$ and $Mg_{12}O_{12}$

The binding affinities for the investigated compounds toward TNF-α receptor and IL-1 receptor targets were evaluated via molecular docking. To determine the inhibition mechanism of TNF-α receptor and IL-1 receptor, CXB-$Zn_{12}O_{12}$ and CXB-$Mg_{12}O_{12}$ complexes were docked in the binding pocket of the targets. The docking results reveal that the CXB-$Zn_{12}O_{12}$ complex (State I) is a potent inhibitor of TNF-α and IL-1 as compared to other compounds. As displayed in Table 6, CXB through NH_2 group interacts with the $Zn_{12}O_{12}$ nanocluster and showed high binding energy in comparison with the CXB-$Mg_{12}O_{12}$ complex as the value of the binding energy of the TNF-α and IL-1 receptors in order were −10.7 and −9.3 kcal/mol. CXB-$Zn_{12}O_{12}$ compound (State I) had a good binding affinity with protein TNF-α through amino acid residues (Tyr119, Leu120, Tyr59, Tyr151, Leu57, and Ile155 and Gly121) from the C chain and also amino acid residues (Tyr151, Leu120, Tyr59, Tyr119, and Gly121) from the D chain by hydrophobic interactions. Hence, the State I was also bounded with other amino acid residues like Ser60, Gln61 and His15 from the C chain and Ser60 from the D chain through polar interactions. Besides, State I bound to amino-acid residue of Tyr59 from the C chain by π-π stacking. Previous study proved that the corresponding amino acid residues (Tyr59, Tyr151, Leu120, Ser60, and Gln61) were important residues in the active site of the target protein (Xu et al., 2018) that exert anti-inflammatory effects through TNF-α inhibition (Fig. 7). Olbert *et al*. experimentally demonstrated zinc oxide nanoparticles at a dose of 14 mg/kg ip decreased the carrageenan-induced paw edema and improved the anti-inflammatory activity of ketoprofen (Olbert et al., 2017). Agarwal *et al*. experimentally showed anti-inflammatory effect of zinc oxide nanoparticles at the concentration of 1 mg/mL by blocking the production and release of inflammatory media-

Table 4 Maximum excitation wavelength (λ_{max}), oscillator strength (*f*) and vertical excitation energies (E) of CXB-$Zn_{12}O_{12}$ complexes in vacuum and aqueous environments.

	E (eV)	λ_{max} (nm)	*f*	Assignment
Vacuum				
I	2.258	549.05	0.0849	H → L + 9(A) (89%)
	2.381	520.53	0.0335	H → L + 6 (48%), H → L + 10 (-29%)
	2.477	500.53	0.0296	H → L + 6 (-21%), H → L + 12 (60%)
II	2.251	550.56	0.0825	H → L + 8 (-14%), H → L + 9 (74%)
	2.44	508.03	0.0296	H → L + 12(A) (70%)
	2.396	517.46	0.0265	H → L + 5(39%), H → L + 6(-17%), H → L + 11
Aqueous				
I	3.582	346.11	0.2049	H → L + 15(10%), H → L + 1(71%)
	4.262	290.88	0.1826	H → L + 19 (25%), H-1 → L + 1(35%)
	2.655	466.96	0.0943	H → L + 4 (–22%), H → L + 6(25%), H → L + 7 (20%), H → L + 8 (11%)
II	3.212	385.91	0.1969	H → L + 1(78%)
	2.192	565.56	0.1231	H → L + 3 (16%), H → L + 4(71%)
	2.414	513.41	0.0479	H → L + 6(82%)

Table 5 Maximum excitation wavelength (λ_{max}), oscillator strength (*f*) and vertical excitation energies (E) of CXB-$Mg_{12}O_{12}$ complexes in aqueous environment.

	E (eV)	λ_{max} (nm)	*f*	Assignment
$Mg_{12}O_{12}$	4.994	248.24	0.0889	H-17 → L (86%)
	4.909	252.78	0.2599	H-14 → L (88%)
	4.231	292.99	0.0057	H-1 → L (93%)
III	3.889	317.94	0.0727	H → L + 16(58%), H-5 → L + 1(2%)
	3.178	390.14	0.1991	H → L + 5(13%), H-1 → L (68%)
	2.255	549.86	0.1098	H → L + 1(76%), H → L + 3(9%)
IV	3.196	387.88	0.0421	H → L + 17(79%), H → L + 1(6%)
	2.281	543.62	0.0125	H → L + 7(65%), H → L + 8(8%)
	1.322	937.70	0.0510	H → L + 1(62%), H → L + 3(27%)

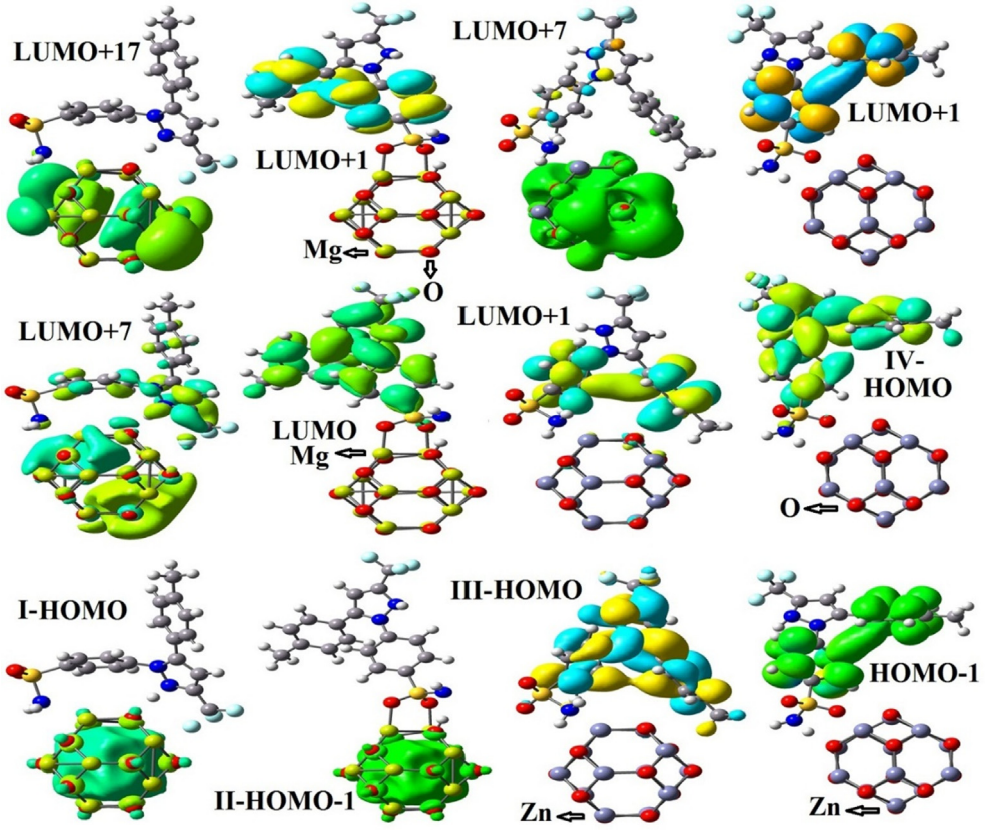

Fig. 6 FMO plots of CXB adsorbed on $Zn_{12}O_{12}$ and $Mg_{12}O_{12}$ nanoclusters in the most stable states.

Table 6 Molecular docking simulations results.

Compound	PDB ID: 2AZ5		PDB ID:2L5X		PDB ID:3RCD	
	BE (kcal/mol)	K_i (μM)	BE (kcal/mol)	K_i (μM)	BE (kcal/mol)	K_i (μM)
ZnO	−6.0	8.6	−4.2	11.1	−6.1	10.3
CXB	−6.3	8.2	−6.1	9.7	−6.3	9.5
I	−10.7	2.4	−9.3	3.7	−9.1	7.5
II	−9.7	3.7	−8.8	4.2	−8.5	8.7
$Mg_{12}O_{12}$	−6.1	8.4	−4.2	11.3	−5.9	10.8
III	−8.5	5.3	−7.6	6.3	−8.8	8.2
IV	−9.8	3.3	−8.1	5.5	−9.7	7.1

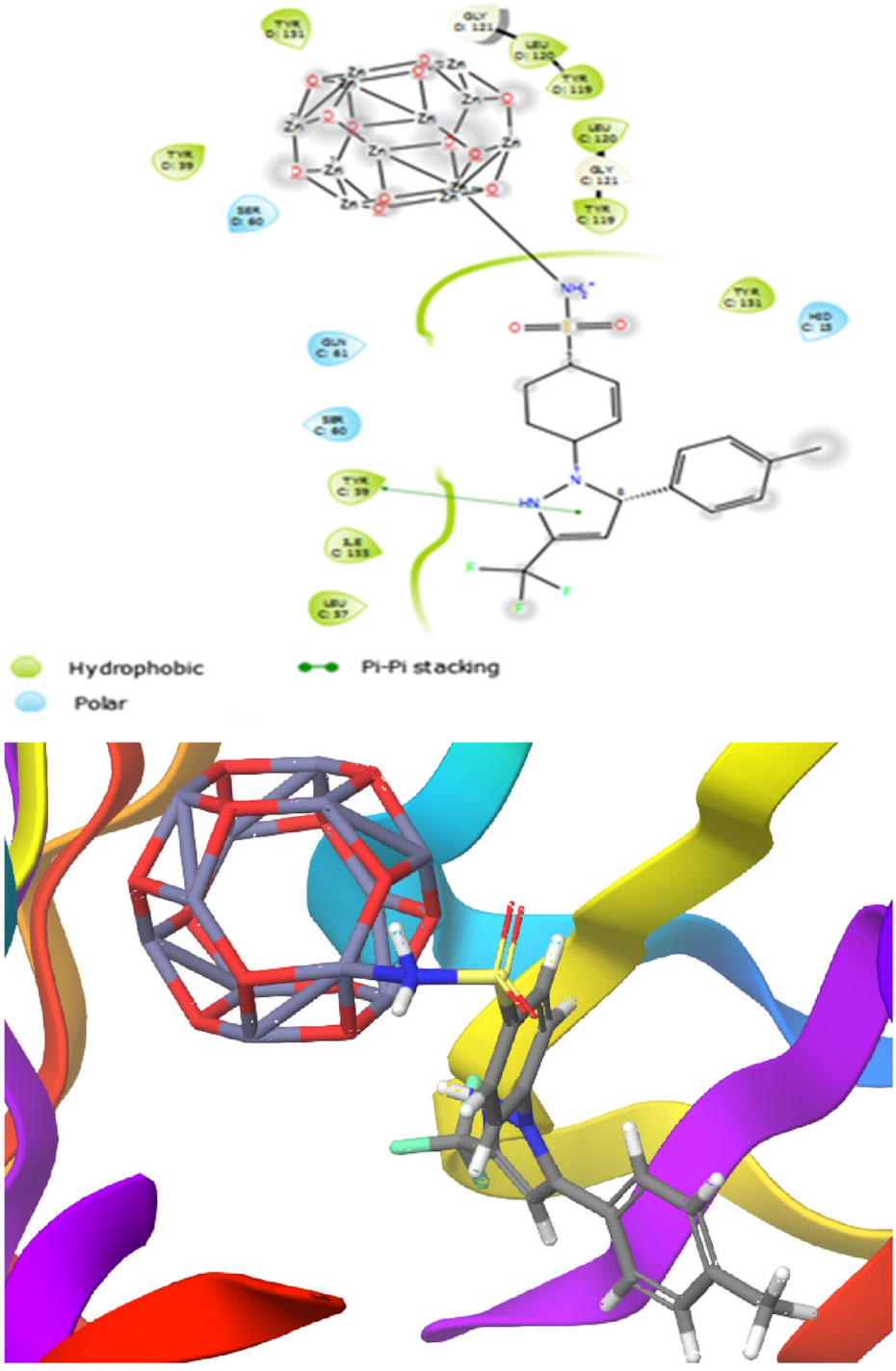

Fig. 7 Presentation of 2D and 3D models of interactions between CXB-$Zn_{12}O_{12}$ complex (State I) and IL-1 receptor (PDB ID: 2LX5).

tors such as IL-1β, IL-6, TNF-α, and COX-2 (Agarwal and Kumar Shanmugam, 2019). The sulfonamide group of State I was stabilized in the binding pocket of IL-1 receptor (PDB ID: 2L5X) in two hydrogen bonds of amino acid residues Thr77 and Arg34. The length of the hydrogen bond distance was 2.39 Å. Hence, the complex was established in the binding pocket of the target by the hydrophobic behavior of amino acid residues (Ala51, Val52, Ile74 and Leu79). In addition, amino acid residues like Asp49, Glu50, Arg34, Lys53, Glu94 and Lys76 bound to the target by electrostatic interactions. The calculations showed that State I bound to the active site consists of amino acid residues like Arg34, Asp49 and Glu50 and lead to the inhibition of the IL-1 receptor (Shokri et al., 2018; Emami et al., 2018). Fig. 7 demonstrates that State I was placed in the active site pocket of the IL-1 receptor. Molecular docking calculations exhibited that State I had a

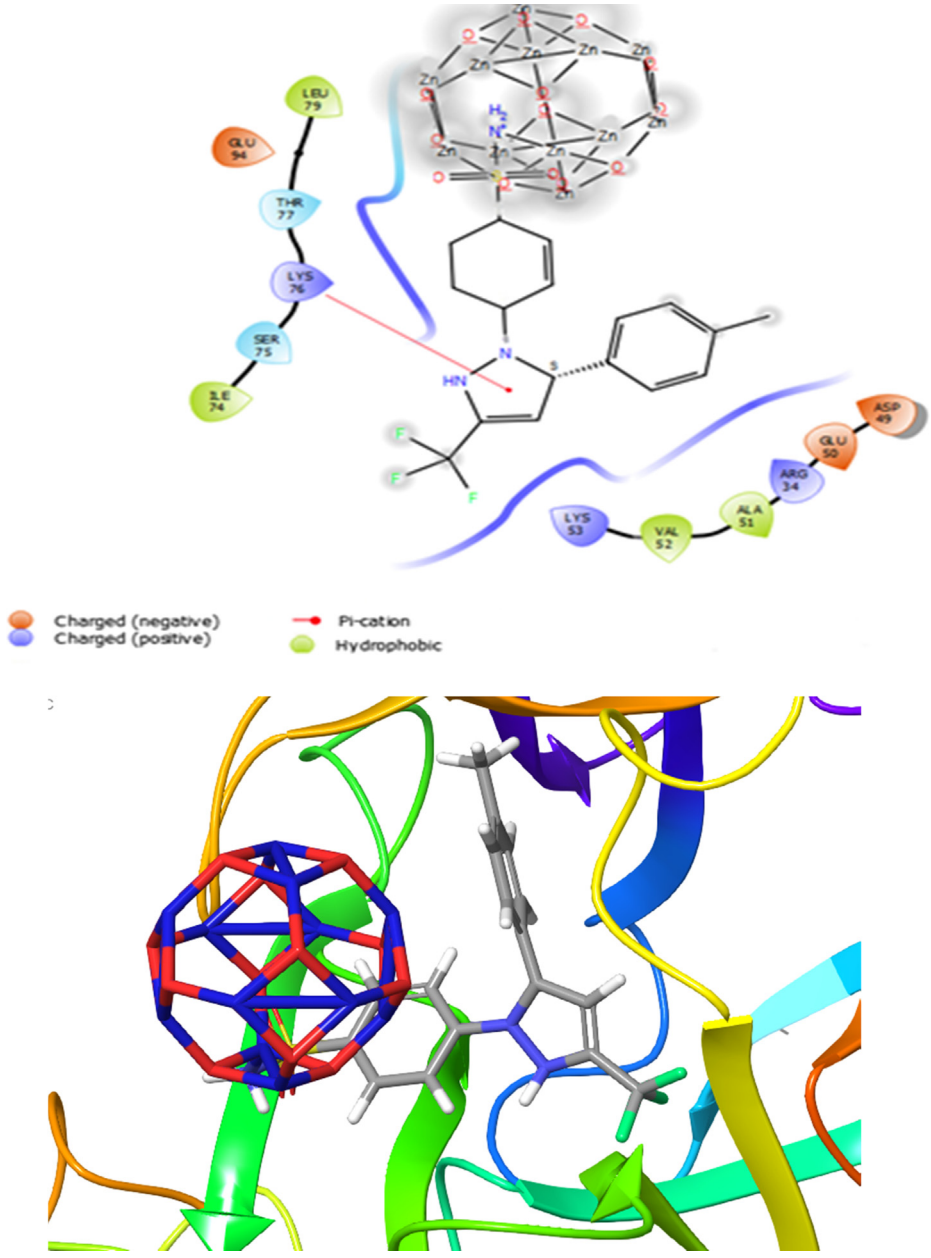

Fig. 8 Presentation of 2D and 3D models of interactions between CXB-$Zn_{12}O_{12}$ complex (State II) and IL-1 receptor (PDB ID: 2LX5).

strong binding affinity to TNF-α and IL-1 receptors and observed that the complex inhibits more influentially the active site of the protein than states II, III, and IV. Therefore, the hydrophobic and hydrogen bond interactions play a crucial role in occupation of the binding pocket. The results demonstrated that CXB/$Zn_{12}O_{12}$ complex (State I) could be considered as promising inhibitors against the TNF-α and IL-1 receptors (see Fig. 8).

Furthermore, to evaluate binding affinity of selected complexes toward human epidermal growth factor receptor 2 (HER2) kinase, molecular docking was done. The aforementioned results revealed that State IV has the lowest binding free energy (−9.7 kcal/mol) compared to other complexes. This binding affinity is well associated with the anticancer activity, where CXB/$Mg_{12}O_{12}$ complex inhibits the HER2 more potently than CXB/$Zn_{12}O_{12}$ complex (Xiang et al., 2017; Mozdoori et al., 2017). Moreover, amino acids residues involved in the active site of the receptor were like Pro945, Cys947, Thr917, Val956, Cys958, Met916, Val912, Arg940, Glu914, Lys887, Ser907, Trp888 and also amino acid residue of Tyr923 interacted with the receptor via hydrogen bond interactions. Therefore, molecular docking simulation exhibited that COX-2 inhibitors could be associated with anticancer properties. Hence, finding of the study illustrated importance of CXB loaded on $Zn_{12}O_{12}$ and $Mg_{12}O_{12}$ nanoclusters for the interaction with the amino acids involved in the binding pocket of HER2 receptor. Accordingly, this compound (State IV) could be developed as potential anticancer compound (El-Azab et al., 2018; Mokhtary et al., 2018).

4. Conclusion

We devised the interaction of CXB through their $–NH_2$ and $–SO_2$ groups on the surface of $Zn_{12}O_{12}$ and $Mg_{12}O_{12}$ nanoclusters in the vacuum and aqueous phases using DFT calculations and molecular docking. The Zn and Mg atoms of $Zn_{12}O_{12}$ and $Mg_{12}O_{12}$ nanoclusters were shown to attract CXB molecules via its positive charge. Our calculation represents that the E_{ads} of CXB is negative in the exothermic process (State II), with values of −1.18 eV (B3PW91) and −1.20 eV (B3LYP) in vacuum phase and −1.38 eV (B3PW91) and −1.26 eV (B3LYP) in aqueous phase. Our calculations demonstrated that CXB from its $–NH_2$ group leads to more changes in the optical and electronic features of the $Zn_{12}O_{12}$ and $Mg_{12}O_{12}$ nanoclusters compared to the $–SO_2$ group. The evaluation of molecular docking represents that State I contain a good binding affinity with these main cytokines (TNF-α and IL-1) as compared with State II, III, and IV.

Declaration of Competing Interest

The authors declare that they have no known competing financial interests or personal relationships that could have appeared to influence the work reported in this paper.

Acknowledgements

- We thank Golestan University of Medical Sciences for providing partial support of the instrumental analysis facilities. The authors want to thank the clinical Research Development Unit (CRDU), Sayad Shirazi Hospital, Golestan University of Medical Sciences, Gorgan, Iran.
- The authors want to thank the Zhejiang Shuren University Basic Scientific Research Special Funds (2020XZ011).

References

Abd El-Mageed, H.R., 2020. Zinc oxide nanoclusters and nanoparticles as a drug carrier for cisplatin and nedaplatin anti-cancer drugs, insights from DFT methods and MC simulation. Mol. Phys. 119, e1842533.

Abdolahi, N., Aghaei, M., Soltani, A., Azmoodeh, Z., Balakheyli, H., Heidari, F., 2018. Adsorption of Celecoxib on $B_{12}N_{12}$ fullerene: Spectroscopic and DFT/TD-DFT study. Spectrochim. Acta, Part A 204, 348–353.

Abdolahi, N., Singla, P., Soltani, A., Javan, M., Aghaei, M., Heidari, F., Sedighi, S., 2020. Gold decorated $B_{12}N_{12}$ nanocluster as an effective sulfasalazine drug carrier: A theoretical investigation. Physica E 124, 114296.

Agarwal, H., Kumar Shanmugam, V., 2019. Synthesis and optimization of zinc oxide nanoparticles using *Kalanchoe pinnata* towards the evaluation of its anti-inflammatory activity. J. Drug Delivery Sci. Technol. 54, 101291.

Aggarwal, D.C., 2006. SHI induced modification of ZnO thin film: Optical and structural studies. Nucl. Instrum. Methods Phys. Res. B 244, 136–140.

Ahmadi Peyghan, A., Baei, M.T., Hashemian, S., 2013. ZnO Nanocluster as a Potential Catalyst for Dissociation of H2S Molecule. J. Clust. Sci., 24, 341-347.

Alalaiwe, A., Carpinone, P., Alshahrani, S., Alsulays, B., Ansari, Mohammed, Anwer, Mohammed, Alshehri, Sultan, Alshetaili, Abdullah, 2019. Influence of chitosan coating on the oral bioavailability of gold nanoparticles in rats. Saudi Pharmaceut. J. 27 (2), 171–175.

Alamdarsaravi, M., Ghajar, A., Noorbala, A.-A., Arbabi, M., Emami, A., Shahei, F., Mirzania, M., Jafarinia, M., Afarideh, M., Akhondzadeh, S., 2017. Efficacy and Safety of Celecoxib Monotherapy for Mild to Moderate Depression in Patients with Colorectal Cancer: A Randomized Double-Blind, Placebo Controlled Trial. Psychiatry Res. 255, 59–65.

Alfaro, A., León, A., Guajardo-Correa, E., Reúquen, P., Torres, F., Mery, M., Segura, R., Zapata, P.A., Orihuela, P.A., 2019. MgO nanoparticles coated with polyethylene glycol as carrier for 2-Methoxyestradiol anticancer drug. PLOS ONE E 14, (8) e0214900.

Ansari, M.J., 2017. Factors Affecting Preparation and Properties of Nanoparticles by Nanoprecipitation Method. Indo Am. J. Pharmaceut. Sci. 4 (12), 4854–4858.

Ansari, M.J., Ahmed, M.M., Fatima, F., Anwer, M.K., Jamil, S., Alshdefat, R., Ali, B.E., Al-Awmi, F., Abdel-Kader, M.S., 2014. solubility and stability enhancement of curcumin through cyclodextrin complexation. Int. J. Biol., Pharm. Allied Sci. 3 (11), 2668–2675.

Ansari, M.J., Ahmed, M.M., Fatima, F., Anwer, M.K., Jamil, S., Alshdefat, R., Ali, B.E., Al-Awmi, F., Abdel-Kader, M.S., 2014. Influence of hydrophilic polymers on complexation and solubilizing efficiencies of beta cyclodextrin over silymarin. Int. J. Biol., Pharm. Allied Sci. 3 (10), 237–242.

Baei, M.T., Ahmadi Peyghan, A., Bagheri, Z., 2013. Quantum chemical analysis on hydrogenated $Zn_{12}O_{12}$ nanoclusters. C. R. Chim. 16, 122–128.

Cai, X., Luo, Y., Zhang, W., Du, D., Lin, Y., 2016. pH-Sensitive ZnO Quantum Dots-Doxorubicin Nanoparticles for Lung Cancer Targeted Drug Delivery. ACS Appl. Mater. Interfaces 8, 22442–22450.

Cao, Y., Khan, A., Balakheyli, H., Ng Kay Lup, A., Taghartapeh, M. R., Mirzaei, H., Khandoozi, S.R., Soltani, A., Aghaei, M., Heidari, F., Sarkar, S.M., Albadarin, A.B., 2021a. Penicillamine functionalized $B_{12}N_{12}$ and $B_{12}CaN_{12}$ nanocages act as potential inhibitors of proinflammatory cytokines: A combined DFT analysis, ADMET and molecular docking study. Arab. J. Chem., 14, 103200.

Cao, Y., Khan, A., Mirzaei, H., Khandoozi, S.R., Javan, M., Ng Kay Lup, A., Norouzi, A., Tazikeh Lemeski, E., Pishnamazi, M., Soltani, A., Albadarin, A.B., 2021b. Investigations of adsorption behavior and anti-cancer activity of curcumin on pure and platinum-functionalized $B_{12}N_{12}$ nanocages. J. Mol. Liquids, 334, 116516.

Cao, Y., Khan, A., Ghorbani, F., Mirzaei, H., Singla, P., Balakheyli, H., Soltani, A., Aghaei, M., Azmoodeh, Z., Aarabi, M., Tavassoli, S., 2021c. Predicting adsorption behavior and anti-inflammatory activity of naproxen interacting with pure boron nitride and boron phosphide fullerene-like cages. J. Mol. Liq. 339, 116678.

Chen, Y., Dong, Y., Du, X., 2020. Lung development: AT1 and AT2 property. Biocell 44 (1), 1.

Chen, X., Sun, Z., Zhang, H., Onsori, S., 2020. Effect of metal atoms on the electronic properties of metal oxide nanoclusters for use in drug delivery applications: a density functional theory study. Mol. Phys. 118, e1692150.

Dastani, N., Arab, A., Raissi, H., 2021. DFT study of Ni-doped graphene nanosheet as a drug carrier for multiple sclerosis drugs. Comput. Theor. Chem. 1196, 113114.

Deng, Z., Liu, C., Zhu, Z., 2021. Inter-hours rolling scheduling of behind-the-meter storage operating systems using electricity price forecasting based on deep convolutional neural network. Int. J. Electr. Power Energy Syst. 125, 106499.

El-Azab, A.S., Abdel-Aziz, A.A.-M., Abou-Zeid, L.A., El-Husseiny, W.M., El_Morsy, A.M., El-Gendy, M.A., El-Sayedd, M.A.-A., 2018. Synthesis, antitumour activities and molecular docking of thiocarboxylic acid ester-based NSAID scaffolds: COX-2 inhibition and mechanistic studies, J. Enzyme Inhib. Med. Chem., 33, 989–998.

Emami, S., Esmaili, Z., Dehghan, G., Bahmani, M., Hashemi, S.M., Mirzaei, H., Shokrzadeh, M., Ershad Moradi, S., 2018. Acetophenone benzoylhydrazones as antioxidant agents: synthesis, in vitro evaluation and structure-activity relationship studies. Food Chem. 268, 292–299.

Fakhar ud Din, Aman, W., Ullah, I., Qureshi, O.S., Mustapha, O., Shafique, S., Zeb, A., 2017. Effective use of nanocarriers as drug delivery systems for the treatment of selected tumors. Int. J. Nanomed. 12, 7291-7309.

Fallahi, P., Jouypazadeh, H., Farrokhpour, H., 2018. Theoretical studies on the potentials of some nanocages ($Al_{12}N_{12}$, $Al_{12}P_{12}$, $B_{12}N_{12}$, $Be_{12}O_{12}$, $C_{12}Si_{12}$, $Mg_{12}O_{12}$ and C_{24}) on the detection and adsorption of Tabun molecule: DFT and TD-DFT study. J. Mol. Liq. 260, 138–148.

Farmanzadeh, D., Keyhanian, M., 2019. Computational assessment on the interaction of amantadine drug with $B_{12}N_{12}$ and $Zn_{12}O_{12}$ nanocages and improvement in adsorption behaviors by impurity Al doping. Theor. Chem. Acc. 138, 11.

Gaussian 09, Revision D.01, M. J. Frisch, G. W. Trucks, H. B. Schlegel, G. E. Scuseria, M. A. Robb, J. R. Cheeseman, G. Scalmani, V. Barone, B. Mennucci, G. A. Petersson, H. Nakatsuji, M. Caricato, X. Li, H. P. Hratchian, A. F. Izmaylov, J. Bloino, G. Zheng, J. L. Sonnenberg, M. Hada, M. Ehara, K. Toyota, R. Fukuda, J. Hasegawa, M. Ishida, T. Nakajima, Y. Honda, O. Kitao, H. Nakai, T. Vreven, J. A. Montgomery, Jr., J. E. Peralta, F. Ogliaro, M. Bearpark, J. J. Heyd, E. Brothers, K. N. Kudin, V. N. Staroverov, R. Kobayashi, J. Normand, K. Raghavachari, A. Rendell, J. C. Burant, S. S. Iyengar, J. Tomasi, M. Cossi, N. Rega, J. M. Millam, M. Klene, J. E. Knox, J. B. Cross, V. Bakken, C. Adamo, J. Jaramillo, R. Gomperts, R. E. Stratmann, O. Yazyev, A. J. Austin, R. Cammi, C. Pomelli, J. W. Ochterski, R. L. Martin, K. Morokuma, V. G. Zakrzewski, G. A. Voth, P. Salvador, J. J. Dannenberg, S. Dapprich, A. D. Daniels, €O. Farkas, J. B. Foresman, J. V. Ortiz, J. Cioslowski, and D. J. Fox, Gaussian, Inc., Wallingford CT, 2009.

Ghenaatian, H.R., Baei, M.T., Hashemian, S., 2013. Zn12O12 nanocage as a promising adsorbent for CS_2 capture. Superlattices Microstruct. 58, 198–204.

Hassanian, M., Aryapour, H., Goudarzi, A., Javan, M.B. Are zinc oxide nanoparticles safe? A structural study on human serum albumin using in vitro and in silico methods. J. Biomol. Struct. Dynam. 39, (1), 330-335

He, J., Han, Y., Xu, G., Yin, L., Ngandeu Neubi, M., Zhou, J., Ding, Y., 2017. Preparation and evaluation of celecoxib nanosuspensions for bioavailability enhancement. RSC Adv. 7, 13053–13064.

Javan, M.B. Magnetic properties of Mg12O12 nanocage doped with transition metal atoms (Mn, Fe, Co and Ni): DFT study. J. Magn. Magn. Mater., 385, 138-144.

Krishnamoorthy, K., Moon, J.Y., Hyun, H.B., Cho, S.K., Kim, S.-J., 2012. Mechanistic investigation on the toxicity of MgO nanoparticles toward cancer cells. J. Mater. Chem. 22, 24610–24617.

Kumari, I., Kaur, N., Gupta, S., Goel, N., 2019. Nucleotide conjugated $(ZnO)_3$ cluster: Interaction and optical characteristics using TDDFT. J. Mol. Graph. Model. 87, 211–219.

Li, Y., Song, K., Cao, Y., Peng, C., Yang, G., 2018. Keratin-Templated Synthesis of Metallic Oxide Nanoparticles as MRI Contrast Agents and Drug Carriers. ACS Appl. Mater. Interfaces 10, 26039–26045.

Lin, L., Xu, M., Mu, H., Wang, W., Sun, J., He, J., Qiu, J.-W., Luan, T., 2019. Quantitative Proteomic Analysis to Understand the Mechanisms of Zinc Oxide Nanoparticle Toxicity to Daphnia pulex (Crustacea: Daphniidae): Comparing with Bulk Zinc Oxide and Zinc Salt. Environ. Sci. Technol. 53, 5436–5444.

Lu, T., Chen, F., 2012. Multiwfn: A multifunctional wavefunction analyzer. J. Comput. Chem. 33, 580–592.

Malarkodi, C., Rajeshkumar, S., Paulkumar, K., Vanaja, M., Gnanajobitha, G., Annadurai, G., 2014. Biosynthesis and Antimicrobial Activity of Semiconductor Nanoparticles against Oral Pathogens. Bioinorg. Chem. Appl. 2014, 1–10.

Mandracchia, D., Tripodo, G., Trapani, A., Ruggieri, S., Annese, T., Chlapanidas, T., Trapani, G., Ribatti, D., 2016. Inulin based micelles loaded with curcumin or celecoxib with effective anti-angiogenic activity. Eur. J. Pharm. Sci. 93, 141–146.

Mirzaei, H., Keighobadi, M., Emami, S., 2017. An overview of anticancer chalcones with apoptosis inducing activity. J. Mazandaran Univ. Med. Sci. 26 (146), 254–268.

Mirzaei, H., Shokrzadeh, M., Emami, S., 2017. Synthesis, cytotoxic activity and docking study of two indole-chalcone derivatives. J. Mazandaran Univ. Med. Sci. 27 (154), 12–25.

Moghri Moazzen, M.A., Borghei, S.M., Taleshi, F., 2012. Synthesis and Characterization of Nano-Sized Hexagonal and Spherical Nanoparticles of Zinc Oxide. J. Nanostruct. 2, 295–300.

Mokhtary, P., Javan, B., Sharbatkhari, M., Soltani, A., Erfani-Moghadam, V., 2018. Cationic vesicles for efficient shRNA transfection in the MCF-7 breast cancer cell line. Int. J. Nanomed. 13, 7107–7121.

Moorthy, S.K., Ashok, C., Rao, K.V., Viswanathan, C., 2015. Synthesis and Characterization of Mgo Nanoparticles by Neem Leaves through Green Method. Mater. Today 2, 4360–4368.

Morris, G.M., Huey, R., Lindstrom, W., Sanner, M.F., Belew, R.K., Goodsell, D.S., Olson, A.J., 2009. AutoDock4 and AutoDockTools4: Automated docking with selective receptor flexibility. J. Comput. Chem. 30 (16), 2785–2791.

Mozdoori, N., Safarian, S., Sheibani, N., 2017. Augmentation of the cytotoxic effects of zinc oxide nanoparticles byMTCP conjugation: Non-canonical apoptosis and autophagy induction inhuman adenocarcinoma breast cancer cell lines. Mater. Sci. Eng., C 78, 949–959.

Nagare, B.J., Chavan, S., Bambole, V., 2017. Study of electronic and optical properties of ZnO clusters using TDDFT method. Mater. Res. Express 4, 106304.

Olbert, M., Gdula-Argasińska, J., Nowak, G., Librowski, T., 2017. Beneficial effect of nanoparticles over standard form of zinc oxide in enhancing the anti-inflammatory activity of ketoprofen in rats. Pharmacol. Rep. 69, 679–682.

Pulay, P., Fogarasi, G., Pongor, G., Boggs, J.E., Vargha, A., 1983. J. Am. Chem. Soc. 105, 7037–7047.

Ravaei, I., Haghighat, M., Azami, S.M., 2019. A DFT, AIM and NBO study of isoniazid drug delivery by MgO nanocage. Appl. Surf. Sci. 469, 103–112.

Revathi, R., Perumal, R.V., Sudharshini, S., Ansar, A.M., Thilagalakshmi, A., Dinesh, A.P., 2011. Simple UV Spectrophotometric Determination of Celecoxib in Pure Form and in Pharmaceutical Formulations. Int. J. Pharmaceut. Sci. Lett. 1 (2), 49–55.

Sharma, D.K., Goyal, A., Chaturvedi, S., 2020. Dietary Inclusions and Exclusions: Preparation Against Cancer. Oncologie 22 (4), 213–224.

Sharma, D., Sabela, M.I., Kanchi, S., Bisetty, K., Skelton, A.A., Honarparvar, B., 2018. Green synthesis, characterization and electrochemical sensing of silymarin by ZnO nanoparticles: Experimental and DFT studies. J. Electroanal. Chem. 808, 160–172.

Shokri, A., Abastabar, M., Keighobadi, M., Emami, S., Fakhar, M., Teshnizi, S.H., Makimura, K., Rezaei-Matehkolaei, A., Mirzaei, H., 2018. "Promising antileishmanial activity of novel imidazole antifungal drug Luliconazole against Leishmania major: in vitro and in silico studies. J. Global Antimicrob. Resistance 14, 260–265.

Soltani, A., Baei, M.T., Tazikeh Lemeski, E., Pahlevani, A.A., 2014. The study of SCN^- adsorption on $B_{12}N_{12}$ and $B_{16}N_{16}$ nano-cages. Superlattices Microstruct. 75, 716–724.

Soltani, A., Ramezani Taghartapeh, M., Erfani-Moghadam, V., Bezi Javan, M., Heidari, F., Aghaei, M., Mahon, Peter J., 2018. Serine adsorption through different functionalities on the $B_{12}N_{12}$ and Pt-$B_{12}N_{12}$ nanocages. Mater. Sci. Eng. C 92, 216–227.

Soltani, A., Khan, A., Mirzaei, H., Onaq, M., Javan, M., Tavassoli, S., Mahmoodi, N.O., Arian Nia, A., Yahyazadeh, A., Salehi, A., Khandoozi, S.R., Khaneh Masjedi, R., Rahman, M.L., Sarjadi, M.

S., Sarkar, S.M., Su, C.-H., 2017. Improvement of anti-inflammatory and anticancer activities of poly(lactic-co-glycolic acid)-sulfasalazine microparticle via density functional theory, molecular docking and ADMET analysis. Arabian J. Chem. 15, 103464.

Tayebee, R., Hosseini-Nasr, A., Zamand, N., Maleki, B., 2015. Density functional study on the adsorption of some aliphatic aldehydes on $(ZnO)_{12}$ and M-doped $(ZnO)_{12}$ nanocages. Polyhedron 102, 503–513.

Vijayakumar, B., Kannappan, V., Sathyanarayanamoorthi, V., 2016. J. Mol. Struct. 1121, 16–25.

Wahab, R., Kim, Y.S., Hwang, I.H., Shin, H.S., 2009. A non-aqueous synthesis, characterization of zinc oxide nanoparticles and their interaction with DNA. Synth. Met. 159, 2443–2452.

Xiang, Z., Yang, X., Xu, J., Lai, W., Wang, Z., Tian, Z.Hu.J., Geng, L., Fang, Q., 2017. Tumor detection using magnetosome nanoparticles functionalizedwith a newly screened EGFR/HER2 targeting peptide. Biomaterials 115, 53–64.

Xu, S., Peng, H., Wang, N., Zhao, M., 2018. Inhibition of TNF-α and IL-1 by compounds from selected plants for rheumatoid arthritis therapy: In vivo and in silico studies. Trop. J. Pharm. Res. 17 (2), 277–285.

Yang, Y., Liu, J., Zhou, X., 2021. A CRISPR-based and post-amplification coupled SARS-CoV-2 detection with a portable evanescent wave biosensor. Biosens. Bioelectron. 190, 113418.

Zhang, L., Xu, Y., Liu, H., Li, Y., You, S., Zhao, J.,... Zhang, J., 2021. Effects of coexisting $Na+$, $Mg2+$ and $Fe3+$on nitrogen and phosphorus removal and sludge properties using A2O process. J. Water Process Eng., (44).

Zhang, X., Tang, Y., Zhang, F., Lee, C., 2016. A Novel Aluminum-Graphite Dual-Ion Battery. Adv. Energy Mater. 6 (11), 1502588.

Zhao, Y., Guo, J., 2021. June). MusiCoder: A Universal Music-Acoustic Encoder Based on Transformer. In: International Conference on Multimedia Modeling, pp. 417–429.

Zhao, W., Wei, J.-S., Zhang, P., Chen, J., Kong, J.-L., Sun, L.-H., Xiong, H.-M., Möhwald, H., 2017. Self-Assembled ZnO Nanoparticle Capsules for Carrying and Delivering Isotretinoin to Cancer Cells. ACS Appl. Mater. Interfaces 9 (22), 18474–18481.